





## Research Article

# Damage Characteristics Caused by Deep-Hole Blasting near Normal Fault and Its Effects on Coal and Gas Outbursts

Kui Gao <sup>1,2</sup>, Guodong Qiao <sup>1</sup>, Zegong Liu <sup>1,2,3</sup> and Wei Xia <sup>1</sup>

<sup>1</sup>School of Safety Science and Engineering, Anhui University of Science and Technology, Huainan, Anhui 232001, China

<sup>2</sup>State Key Laboratory of Mining Response and Disaster Prevention and Control in Deep Coal Mines, Anhui University of Science and Technology, Huainan, Anhui 232001, China

<sup>3</sup>Key Laboratory of Mine Safety and Highly Efficient Mining Jointly Built by Province and Education Ministry, Anhui University of Science and Technology, Huainan, Anhui 232001, China

Correspondence should be addressed to Guodong Qiao; [guodongqiao123@163.com](mailto:guodongqiao123@163.com) and Wei Xia; [1368477854@qq.com](mailto:1368477854@qq.com)

Received 7 January 2022; Revised 29 January 2022; Accepted 17 March 2022; Published 13 April 2022

Academic Editor: Xuelong Li

Copyright © 2022 Kui Gao et al. This is an open access article distributed under the Creative Commons Attribution License, which permits unrestricted use, distribution, and reproduction in any medium, provided the original work is properly cited.

To understand the stability of coal and rock in areas of normal faults disturbed by the dynamic loads of blasting, the damage characteristics of coal and rock within a normal fault are investigated using similarity simulation tests. The mechanism for coal and gas outbursts within a normal fault is analyzed theoretically, and the results indicate that the maximum tensile stress in the vertical direction of the blasting hole in the normal-fault model is 1.17 times that in the no-fault model. The propagation of cracks near the blasting hole produces crushing circles, and more cracks are produced in the normal-fault model, causing severe damage to the coal seam and floor rock adjacent to the upper wall of the normal fault. Meanwhile, coal on the surface of the coal seam falls off. The cracks extend to the roof rock through the footwall of the normal fault. Cracks in the adjacent strata and coal seam interpenetrate those around the blasting hole, which is a potentially dangerous area for coal and gas outbursts. The cumulative damage caused by blasting vibrations increases the extent and scope of the damage to coal and rock, and broken coal and rock provide weak surfaces and gas flow channels that can lead to dynamic gas disasters. The research results will provide a theoretical basis for gas dynamic disasters induced by blasting disturbance in normal fault structures. Based on cases of coal and gas outbursts in the Didaoshenghe Coal Mine in Heilongjiang Province, China, an important reason for such incidents is considered to be the blasting areas of normal faults being disturbed by air-powered coal drilling.

## 1. Introduction

A coal and gas outburst is a complicated dynamic disaster [1]. Generally, an outburst lasts for only a matter of seconds from initiation to termination [2, 3], but during that time, anything from hundreds to tens of thousands of tons of coal are ejected from the coal wall onto adjacent roadways, with large amounts of gas also discharged [4–6]. Outbursts occur mainly in local areas of mined coal seams and generally near geological structural zones [7–10]. Comparing the frequency and proportion of gas outbursts between the normal fault and the upper wall of the fault, it is found that the gas outburst controlled by the fault occurs mainly on the upper wall of the normal fault and is located mainly within 20 m of the fault plane. The outburst strength of the upper wall is also

much greater than that of the footwall [11]. Deep-hole blasting technology is being used increasingly in coal mines [12]. In recent years, coal and gas outburst disasters caused by blasting operations have occurred from time to time in geological structure areas [13]. Many scholars have studied the damage and physical state changes of coal and rock mass under different conditions [14–16]. Some scholars use electromagnetic radiation, the microseismic, and other means to study the failure characteristics of coal and rock masses [17–19]. The effects of blasting on the stability of coal and rock within a structural area have not been investigated previously [20, 21]. To date, no in-depth study has been performed on the damage and failure characteristics of coal within structural areas under explosion load [22, 23]. The aim of the present study is to investigate the damage

characteristics of coal and rock under the action of a dynamic blasting load within a normal fault and their influence on dynamic outburst disasters by combining similarity experiments, numerical simulations, and theoretical analyses.

## 2. Simulation Experiment of Blasting in Normal Fault

**2.1. Simulated Experimental Device.** The model followed the Froude proportional method and was created in the laboratory [23].

$K_\rho \in (1.24, 1.6)$ ,  $K_\sigma \in (0.15, 0.4)$ , and  $K_l = K_\sigma/K_\rho = (0.15/1.6, 0.4/1.24) = (0.09, 0.32)$ . The sample used in this experiment was tectonic soft coal. According to the value range of the stress ratio,  $K_\sigma$  is 0.4 and  $K_\rho$  is 1.6. Thus,  $K_l = K_\sigma/K_\rho = 0.25$ .

The interior dimensions of the box housing the experimental device were 30 cm × 30 cm × 30 cm. The front and back sides of the box were made of detachable steel plates sealed by high-strength silicone pads and bolts. The connection between the loading device and the main box body was sealed with a sealing ring, and the box body was inflated via a high-pressure gas cylinder, which made the conditions of the model test more consistent with those in the field. The main parts of the loading device were three hydraulic jacks, three pressure-transmission steel plates, and one pressure-transmission device, as shown in Figure 1.

**2.2. Stress Monitoring System.** An AFT-0957-8 superdynamic strain data acquisition system was used to collect the strain values of strain bricks in three different directions during the blasting process in real time. The experimental data monitoring system and strain bricks are shown in Figure 2.

For the plane stress model, according to the strain value, the stress value of the corresponding measuring point can be calculated as

$$\sigma = \frac{E}{2(1-\mu)}(\varepsilon_1 - \varepsilon_3) \pm \frac{E}{2(1+\varepsilon)} \sqrt{(\varepsilon_1 - \varepsilon_3)^2 + (2\varepsilon_2 - \varepsilon_1 - \varepsilon_3)^2}, \quad (1)$$

where  $\sigma$  is the stress,  $\varepsilon_1$  is the horizontal strain,  $\varepsilon_2$  is the strain at 45°,  $\varepsilon_3$  is the vertical strain, and  $E$  (GPa) is the elastic modulus.

**2.3. Preparation of Experimental Cartridge.** The experimental cartridge was made from a PVC tube with a diameter of 16 mm and a thickness of 1 mm. A second-level permissible water gel explosive used in coal mines was inserted into the cartridge for the experiment, and a special detonating fuse equal to the length of the PVC tube was placed in the cartridge tube. A detonator was used to detonate the explosive, as shown in Figure 3. After the cartridge was made, antistatic paint was smeared on the outer wall of the PVC tube.

### 2.4. Construction of Experimental Model

**2.4.1. Design.** As shown in Figure 4, the rock layer contains a blasting hole 15 cm from the left edge of the model and

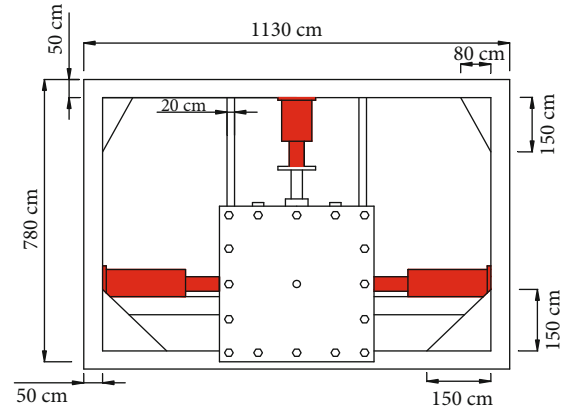


FIGURE 1: Schematic of experimental blasting device.

10 cm from the bottom surface, and the thickness of the coal layer is 4 cm. A test model with no normal fault was also designed as a control.

As shown in Figure 5, stress measuring points 3 and 4 are directly above the blasting hole at distances of 3 cm and 5 cm, respectively; in the horizontal direction, stress measuring points 1 and 2 are 3 cm and 5 cm, respectively, from the blasting hole. The superdynamic strain data acquisition instrument was used to record the strain data of the blasting in real time, and the stresses at the corresponding measuring points were calculated from the strain values.

**2.4.2. Process for Making Experimental Model.** The experimental prototype was working face 14136 of the sixth coal seam of the Zhangji mine in the Huainan mining area. This working face contains 14 faults, five of which have a drop of greater than 3 m and nine of which have a drop of less than 3 m. The original mechanical parameters of the coal and rock are given in Table 1 (original mechanical parameters of coal and rock) [24]. The material ratio parameters of the experimental model are given in Table 2 (material ratio parameters) [24–26], and the hardness of the fault plane is less than that of the normal rock layer.

The test model was formed in a prefabricated wooden box, and the fault plane was preplaced using cardboard. The strain bricks and the blasting hole were embedded at the corresponding positions according to the design of the model, as shown in Figure 6(a). The test model was maintained at room temperature for one month and then unpacked after air drying, as shown in Figures 6(b) and 6(c). For the test, the model was loaded into the blasting simulation test device, and a blasting cartridge was placed in the blasting hole and then sealed, as shown in Figure 6(d).

The completed test system is shown in Figure 7 [26, 27]. Finally, the sealed test device was filled with CO<sub>2</sub>, and the detonator and exploder were connected for the blasting simulation test.

**2.5. Analysis of Experimental Results.** The growth of cracks in the experimental models after blasting is shown in Figure 8. In both models, all the blasting cracks extend along the blast hole.

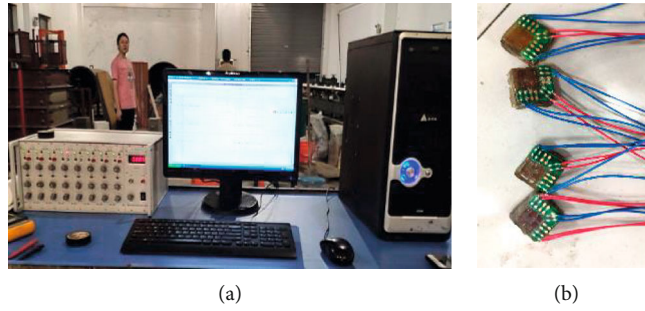


FIGURE 2: Experimental data monitoring system and strain bricks: (a) test data monitoring system; (b) strain bricks.

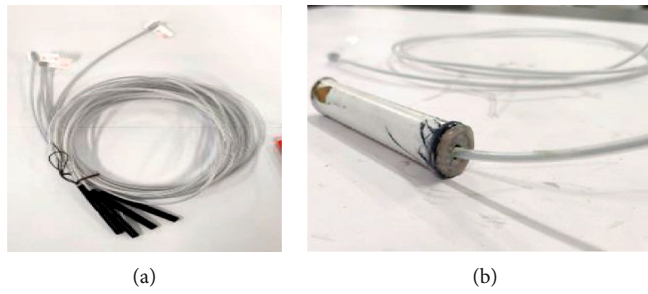


FIGURE 3: Experimental cartridge: (a) detonator; (b) blasting cartridge.

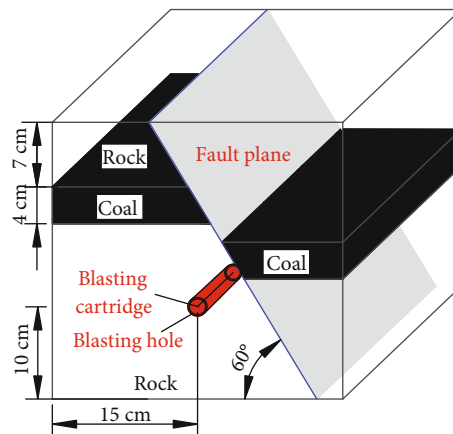


FIGURE 4: Experimental blasting test model.

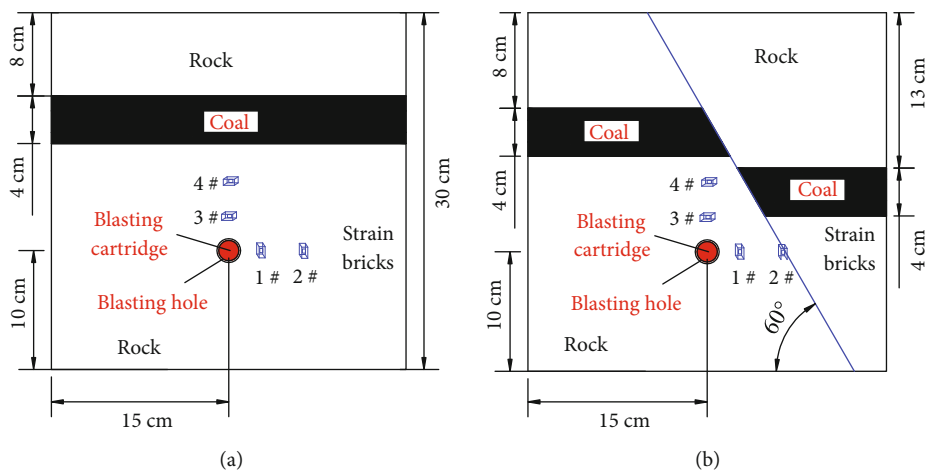


FIGURE 5: Layout of stress measuring points used in blasting test: (a) model with no normal fault; (b) model with normal fault.

TABLE 1: Original mechanical parameters of coal and rock [24].

Rock type	Density (g/cm <sup>3</sup> )	Modulus of elasticity (GPa)	Poisson's ratio	Compressive strength (MPa)	Tensile strength (MPa)
Mudstone	2.4	9.8	0.24	28.2	1.3
Coal seam	1.4	5.3	0.32	7.1	0.4

TABLE 2: Material ratio parameters [24].

Rock type	Sand	Cement	Gypsum	Water	Coal
Rock	6.1	1.2	0.5	0.70	0
Coal seam	2.5	0.2	1.2	0.65	1.8

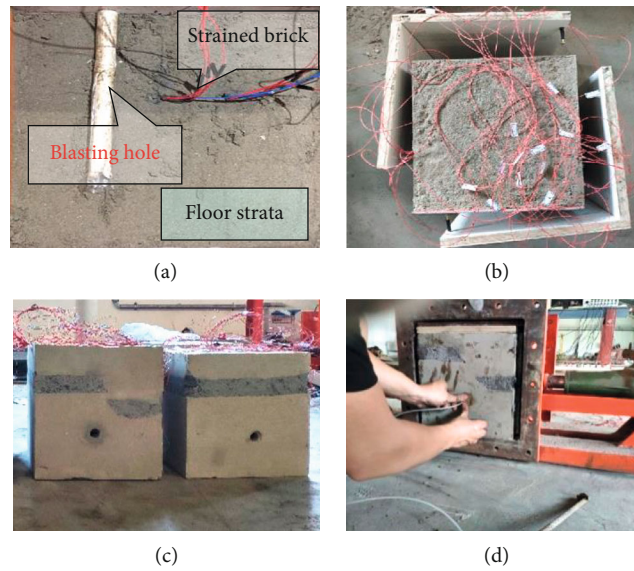


FIGURE 6: Development of experimental model: (a) floor strata laying of normal fault floor; (b) form stripping; (c) completion of experimental model; (d) charge and sealing.

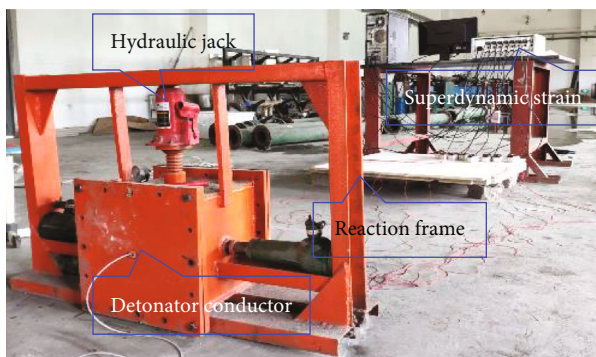


FIGURE 7: Experimental system of blasting simulation.

The model with no normal fault is shown in Figure 8(a). When the blasting stress wave propagates from the rock to the coal seam, many blasting cracks appear in the rock between the blast hole and the underside of the coal seam; this phenomenon can be explained by the theory that the explosive stress wave destroys the medium. The model with a normal fault is shown in Figure 8(b). The cracks around the blast hole develop asymmetrically. The coal-rock inter-

face and the coal seam are seriously damaged, and the upper wall and footwall coal seams are peeled off. The internal damage of the coal body is serious. The cracks extend to the upper wall of the fault, and the blasting stress wave continues to propagate through the coal seam at the footwall of the fault. After passing through the coal seam and encountering the roof rock, the damage of the roof rock is intensified, and the cracks extend into the roof rock.

By comparison, it can be seen that the normal fault structure and the fault plane are affected greatly by the dynamic blasting disturbance, and the coal and rock layers near the upper wall of the blast hole are disturbed most strongly by the blasting stress. Because of the repeated accumulation of blast vibrations and the presence of the normal fault structure, the destruction of the rock and coal seam near the upper-wall coal seam of the fault has been accelerated, and the coal and rock in the area of the normal fault structure have been weakened.

From the strain values monitored by the embedded strain bricks, the stresses at the corresponding measuring points can be calculated. The stress curves for the measuring points are displayed in Figures 9 and 10. Positive values represent compressive stress produced by compressive stress

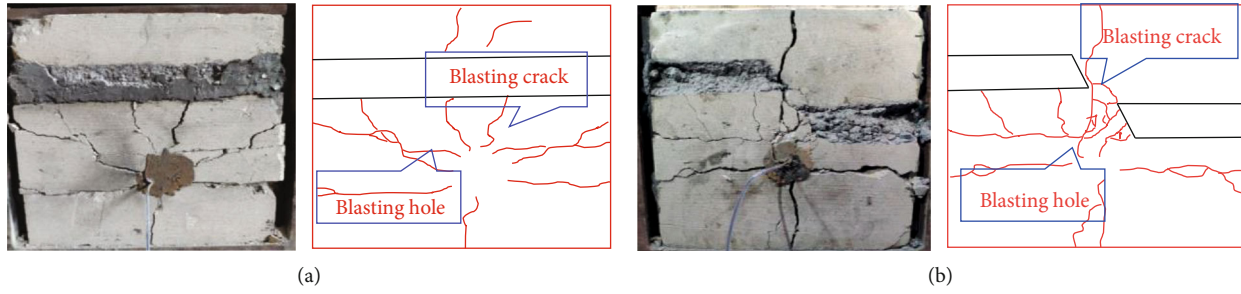


FIGURE 8: Crack development within models after blasting: (a) cracks in model with no fault after blasting; (b) cracks in model with normal fault after blasting.

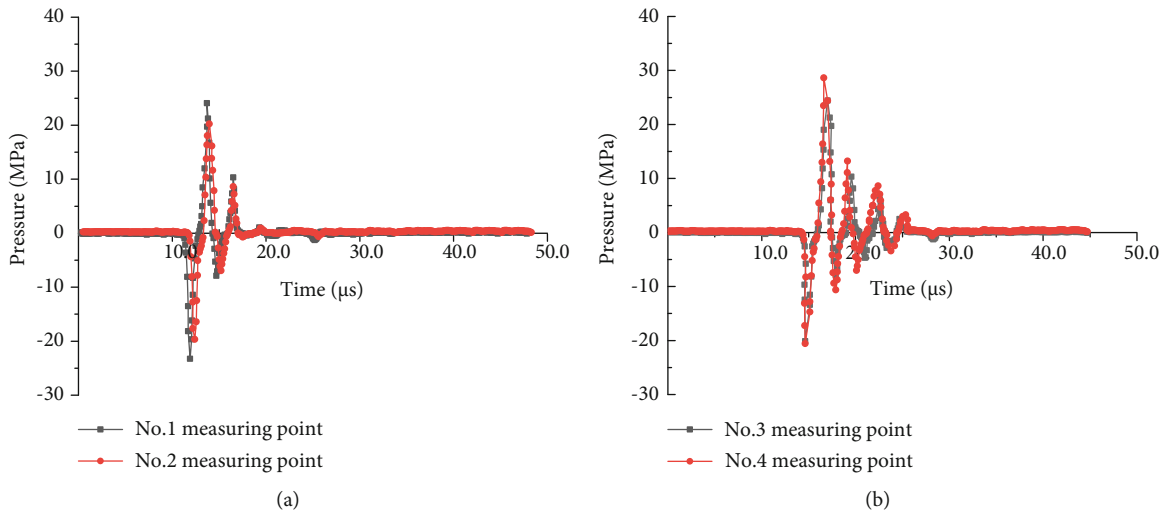


FIGURE 9: Stress variation curves of experimental model with no normal fault: (a) measuring points 1 and 2; (b) measuring points 3 and 4.

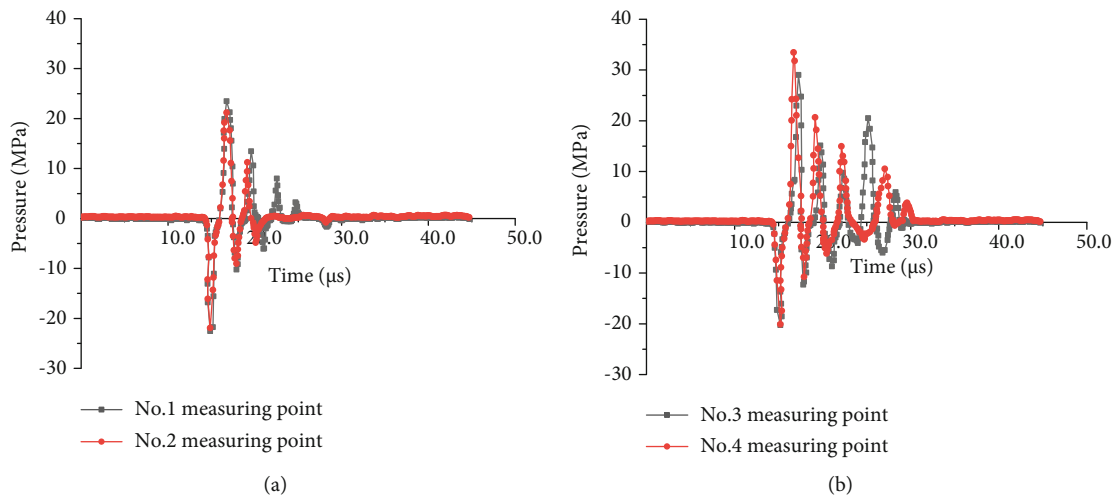


FIGURE 10: Stress variation curves of experimental model with normal fault: (a) measuring points 1 and 2; (b) measuring points 3 and 4.

waves, and negative values represent tensile stress produced by tensile stress waves.

In Figure 9, the trend for the stress at measuring point 1 is similar to that at measuring point 2. They both reach the peak of compressive stress and then the peak of tensile stress. The maximum tensile and compressive stress peaks are not

much different. The acting time of stress at measuring points 3 and 4 is longer than that at measuring points 1 and 2, and the maximum tensile stress is greater than the maximum compressive stress. Taking measuring point 4 as an example, the maximum tensile stress is 28.6 MPa, the maximum compressive stress is 20.1 MPa, and the maximum tensile stress is

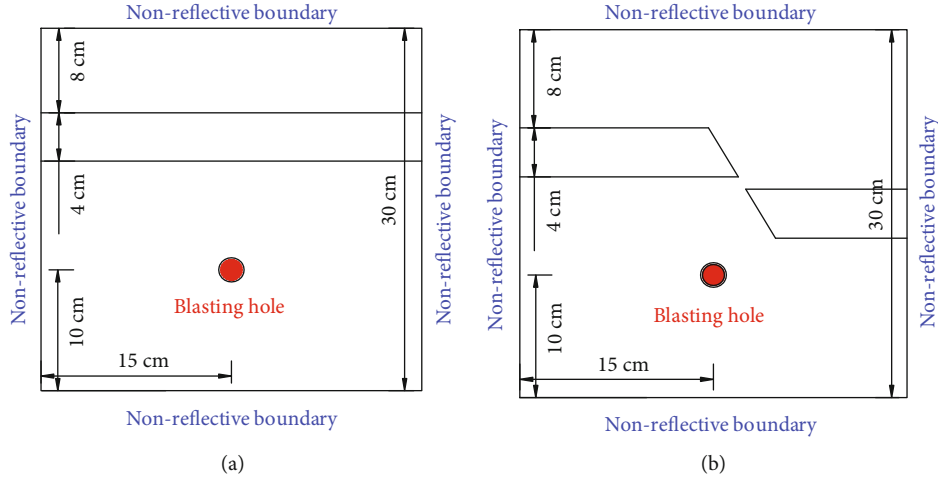


FIGURE 11: Numerical simulation models: (a) with no normal fault; (b) with normal fault.

1.42 times the maximum compressive stress. The maximum tensile stress at measuring point 4 is 1.19 times that at measuring point 1 and 1.35 times that at measuring point 2.

The data in Figure 10 show that the stresses recorded at measuring points 1 and 2 have similar trends. They both reach the maximum compressive and tensile stresses successively and then tend to reduce gradually to zero over time. The stress curves at measuring points 3 and 4 show multiple stress peaks after reaching the maximum compressive and tensile stresses. As time goes by, the peaks gradually become smaller. Because of the presence of the upper-wall and foot-wall coal seams of the normal fault, the blasting stress wave is reflected at the coal-rock interface to form a tensile stress wave, and a stress concentration forms at measuring point 3. So, at  $25.2 \mu\text{s}$ , there is a larger stress peak at measuring point 3, which reaches 20.5 MPa.

Comparing Figures 10(a) and 10(b) shows that the maximum stresses at measuring points 3 and 4 are obviously larger than those at measuring points 1 and 2. Because of the presence of the normal fault, the blasting stress wave is reflected and transmitted at the coal-rock interface, and a reflected tensile stress wave and transmitted compressive stress wave appear, resulting in blasting stress concentration. The maximum tensile stress at measuring point 4 is 33.5 MPa, which is 1.39 times that at measuring point 1 and 1.65 times that at measuring point 2. The maximum tensile stress at measuring point 3 is 29.1 MPa, which is 1.21 times that at measuring point 1 and 1.43 times that at measuring point 2.

Comparing the stress changes of the two experimental models shows that the maximum tensile stress in the vertical direction of the blast hole in the normal-fault model is 1.17 times that in the model with no normal fault. The change of the stress curve in the vertical direction of the blast hole in the normal-fault model is obviously more complicated, and the action time is longer. Because of the presence of the normal fault, the stress at measuring point 3 suddenly reaches high tensile stress during the stress decay process. The stress wave produces multiple transmissions and reflec-

tions in the normal-fault structural area, which cause serious damage to the coal-rock interface.

### 3. Numerical Simulation of Blasting in Normal Fault

According to the relevant parameters of the experimental model, the ANSYS/LS-DYNA numerical simulation software was used to establish a numerical model to explore further the stress states with and without a normal fault under blasting loads.

*3.1. Construction of Numerical Model.* Numerical simulation analyzes the finite-field problem. To eliminate the effects of boundary reflections on the explosion stress wave, the numerical model was given nonreflective boundaries. The established numerical model is shown in Figure 11 and involves coal, rock, and blasting gas, thereby giving rise to a typical fluid-solid coupling problem. LS-DYNA uses a simplified arbitrary Lagrangian-Eulerian algorithm that combines the Lagrangian and Eulerian methods to analyze the fluid-solid coupling problem of blasting in coal and rock.

The coal and rock mechanical parameters used in the numerical simulation are the same as those used in the similarity simulation experiment. The original mechanical parameters of the numerically simulated materials are shown in Table 1. The Jones-Wilkins-Lee equation of state is used to describe the pressure and volume of the detonation products [28], i.e.,

$$P = A \left( 1 - \frac{\omega}{R_1 V} \right) e^{-R_1 V} + B \left( 1 - \frac{\omega}{R_2 V} \right) + \frac{\omega E_0}{V}, \quad (2)$$

where  $P$  (MPa) is the pressure of the detonation products,  $A$  and  $B$  (GPa) are explosive parameters,  $R_1$ ,  $R_2$ , and  $\omega$  (dimensionless) are explosive parameters,  $E_0$  (MJ) is the internal energy generated by the detonation products, and  $V$  ( $\text{m}^3$ ) is the relative volume of the detonation products.

TABLE 3: Parameters of explosive material.

$\rho$ (kg/m <sup>3</sup> )	$D$ (m/s)	$A$ (GPa)	$B$	$R_1$	$R_2$	$\omega$	$E_0$ (GPa)
950	2800	347	7.33	4.15	0.95	0.3	2

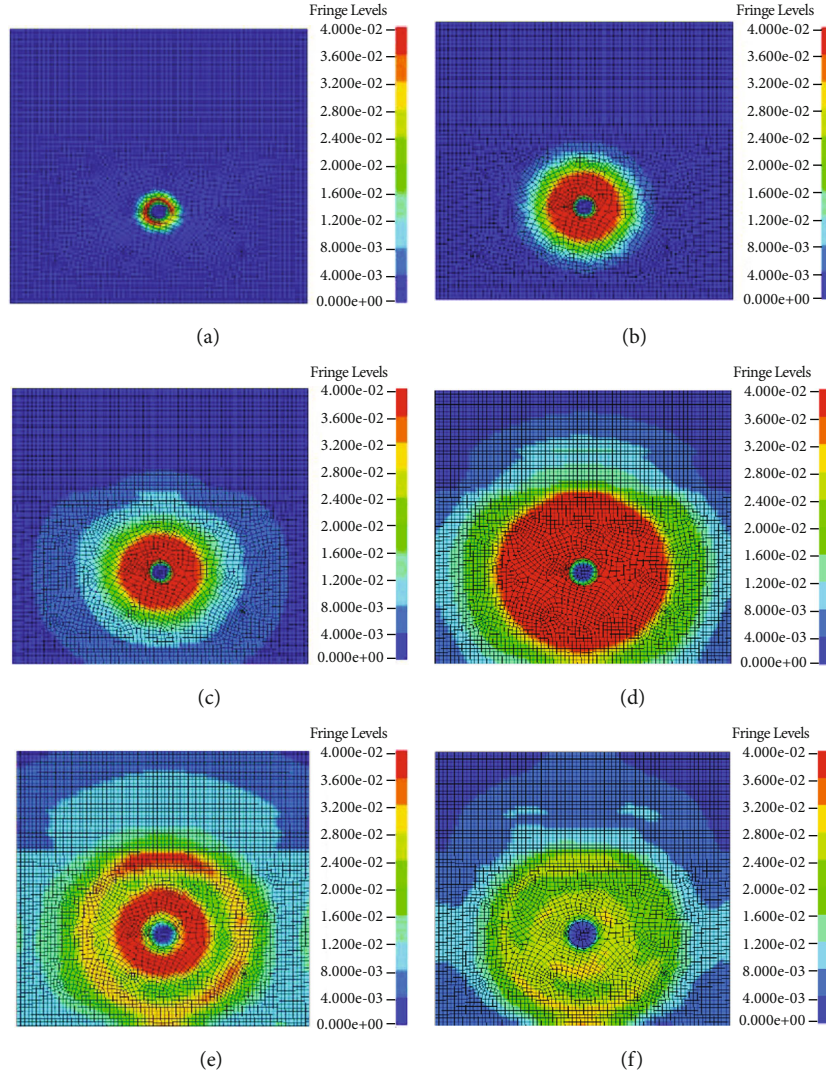


FIGURE 12: Stress clouds for numerical model with no normal fault at different moments:  $t =$  (a)  $5 \mu\text{s}$ , (b)  $10 \mu\text{s}$ , (c)  $15 \mu\text{s}$ , (d)  $20 \mu\text{s}$ , (e)  $25 \mu\text{s}$ , and (f)  $40 \mu\text{s}$ .

The density of the explosive material is  $950 \text{ kg/m}^3$ , and its detonation velocity is  $2800 \text{ m/s}$ . The parameter settings of the explosive used in the numerical calculations are given in Table 3.

**3.2. Analytical Results.** Stress cloud diagrams of the no-fault numerical model at different times are shown in Figure 12. These simulations show that at  $t = 5 \mu\text{s}$ , a uniform stress nephogram appears around the blasting hole. At  $t = 15 \mu\text{s}$ , the stress wave propagates into the coal seam. At  $t = 25 \mu\text{s}$ , the blasting stress wave is transmitted and reflected upon reaching the coal-rock interface. An obvious stress concentration appears directly below the line connecting the coal seam and the blasting hole; this can explain why the tensile

stress peaks at measuring points 3 and 4 are obviously greater than the compressive stress peaks in the similarity simulation test.

The stress cloud diagram of the numerical model with the normal-fault structure is shown in Figure 13. These show that at  $t = 5 \mu\text{s}$ , the blasting stress wave propagates uniformly along the hole during its initial development, and the stress is less affected by the normal fault. At  $t = 15 \mu\text{s}$ , stress concentration occurs in the rock between the two coal seams. This corresponds to the larger stress peaks in Figures 10(a) and 10(b) and the conversion between compressive stress and tensile stress that occurred multiple times, resulting in more cracks in the normal fault near the upper wall and footwall area after blasting. At  $t = 25 \mu\text{s}$ , the propagation of

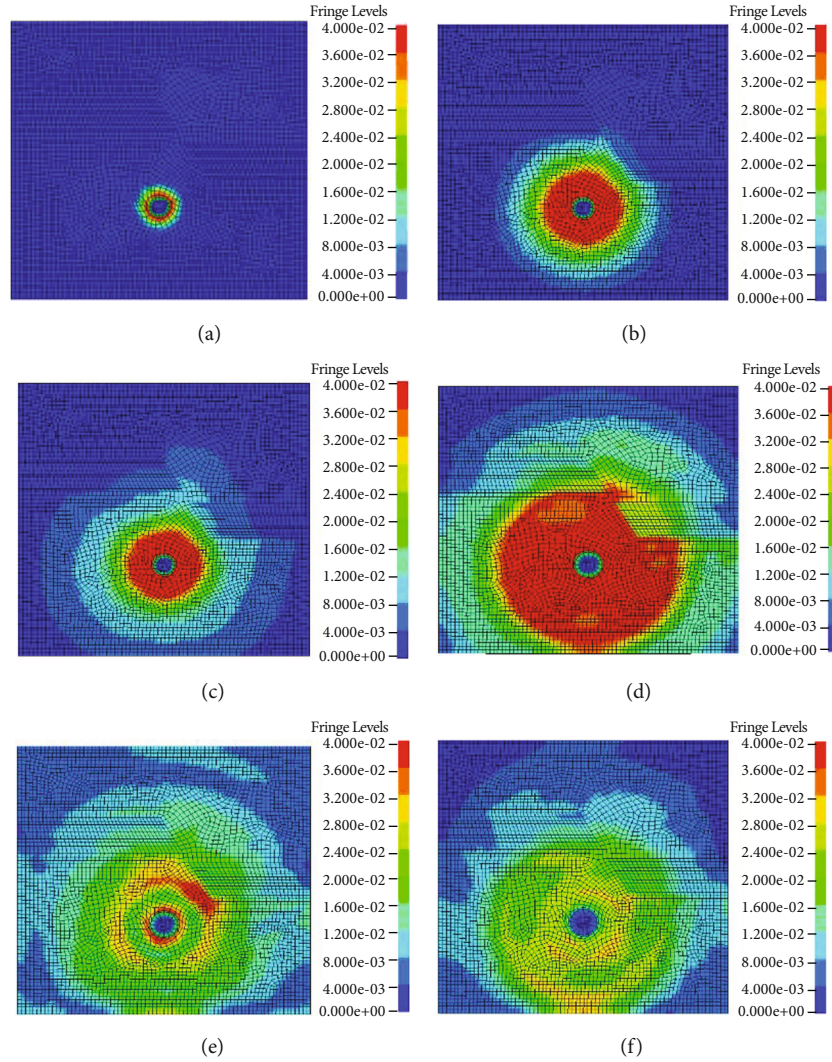


FIGURE 13: Stress clouds for numerical model with normal fault at different moments:  $t =$  (a)  $5 \mu\text{s}$ , (b)  $10 \mu\text{s}$ , (c)  $15 \mu\text{s}$ , (d)  $20 \mu\text{s}$ , (e)  $25 \mu\text{s}$ , and (f)  $40 \mu\text{s}$ .

the blasting stress is relatively complicated, with an obvious stress concentration on the fault plane of the coal body in the upper wall of the normal fault. This corresponds to the complicated stress-state changes at measuring points 3 and 4 in the blasting simulation test of the normal-fault model, exacerbating the damage to both coal and rock.

#### 4. Causes of Coal and Gas Outburst near Normal Fault Disturbed by Blasting

*4.1. Analysis of Influence of Normal Fault on Coal Structure.* The dynamic force exerted by a normal fault comes from either the vertical movement of the Earth's crust or the weight of the rock strata. The means of action of crustal movement or the weight of the rock strata is that a vertically downward maximum principal stress is generated above the rupture surface of the normal fault, resulting in shear deformation of the fault plane. It is assumed that the weight of the rock strata provides a power source for the formation of a

normal fault, and the triaxial stress state of a normal fault is shown in Figure 14. According to the fault model proposed by Anderson [29], the studied rock is regarded as an isotropic body. A normal fault is controlled by three principal stresses, i.e.,  $\sigma_1$ ,  $\sigma_2$ , and  $\sigma_3$ , where  $\sigma_1$  is the maximum principal stress,  $\sigma_2$  is the intermediate principal stress, and  $\sigma_3$  is the minimum principal stress.

When the normal-fault rupture surface is formed,  $\sigma_1$  plays a major role, so the two-dimensional stress is analyzed next. It is assumed that the initial state of the rock layer is horizontal and that the dip angle of the normal fault is  $\alpha$ , and the stress state on the fault surface is analyzed [29]. The two-dimensional stress diagram is shown in Figure 15.

When the fault dip is consistent with rock-strata dip, the dip angle of the rock is set as  $\varphi$  and that of the fault plane is set as  $\alpha$ . The angle between the rock and the horizontal direction is set as  $\theta$ . There is an acute angle between the rock and the fault, with  $\alpha = \theta + \varphi$ . For a single homogeneous rock layer, when the vertical compression pressure that causes the



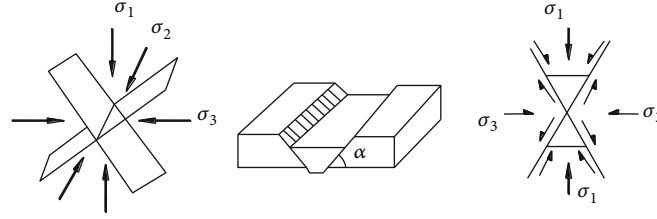


FIGURE 14: Triaxial stress state of normal fault.

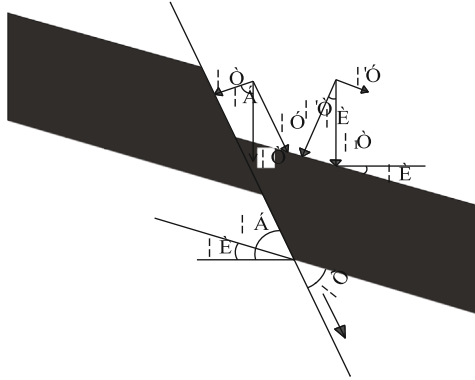


FIGURE 15: Schematic of mechanical analysis in hanging wall of normal fault.

fault is  $\sigma_1$ , there is a positive pressure  $\sigma$  and a shear  $\tau$  on the fault plane, where

$$\left. \begin{aligned} \sigma &= \sigma_1 \cos \alpha = \sigma_1 \cos (\theta + \varphi) \\ \tau &= \sigma_1 \sin \alpha = \sigma_1 \sin (\theta + \varphi) \end{aligned} \right\} \quad (3)$$

When the rock layer is inclined,  $\sigma_1$  can be divided into  $\sigma'$  and  $\tau'$  on the rock layer, where

$$\sigma' = \sigma_1 \cos \theta, \tau' = \sigma_1 \sin \theta. \quad (4)$$

From Equations (3) and (4), we obtain

$$\tau' = \frac{\tau \sin \theta}{\sin (\theta + \varphi)}. \quad (5)$$

After the fault is formed, the development directions of the main fault and the secondary shear fracture surface are determined by the directions of  $\tau$  and  $\tau'$ , respectively, and the damage width and extent are determined by the stresses  $\tau$  and  $\tau'$ .

- (1) When  $\theta = 0$ , we have  $\alpha = \varphi$ ,  $\tau = \sigma_1 \sin \alpha$ , and  $\tau' = 0$ , which shows that when the rock layer is level, the shear component of  $\sigma_1$  acting on the rock layer is  $\tau' = 0$ , and the rock layer is affected only by the vertical pressure, with no shear along the rock layer. However, on the existing fault plane, we have  $\tau \neq 0$ , which causes the upper wall to slide down along the section, forming a parallel-section secondary

shear joint on the upper wall and developing into a parallel-section failure zone

- (2) When  $\theta \neq 0$ , there are shear components  $\tau$  and  $\tau'$  of  $\sigma_1$  on both the fault plane and the rock plane. When  $\sigma_1$  is constant, the values and directions of  $\tau$  and  $\tau'$  are determined by  $\varphi$  and  $\theta$ . The fault dip angle  $\alpha$  remains unchanged, as does  $\tau$ ; meanwhile,  $\tau'$  increases with increasing  $\theta$ , thereby exacerbating the tendency of the upper wall of the fault to slide along the coal seam, which can cause a wider structural coal belt to form. With increasing  $\theta$ , when  $\theta = \alpha$ , we have  $\varphi = 0$  and  $\tau' = \tau \sin \theta / \sin (\theta + \varphi) = \tau$ , which can cause large-scale faults to form parallel to the coal seam
- (3) When  $\theta$  does not change,  $\tau'$  is constant and  $\tau$  decreases as  $\varphi$  decreases. When  $\varphi = 0$ , we have  $\tau' = \tau \sin \theta / \sin (\theta + \varphi) = \tau$ , and a large-scale coal-seam fault can form in the upper wall

In summary, when the fault dip is consistent with the rock dip, the effective shear stresses  $\tau$  and  $\tau'$  are concentrated in the upper-wall rock of the fault, and an upper-wall failure zone forms. The scale of the failure zone and the extent of the damage are determined by the angle  $\varphi$  between the fault plane and the rock layer. In the inclined rock, the smaller  $\varphi$ , the wider the upper-wall failure zone and the greater the coal destruction.

Under the failure action of shear stress at the normal-fault plane, the coal and rock around the fault plane are destroyed, and there emerge small faults parallel to the main plane and associated joints that intersect the main plane. As the structural stress continues to act on the upper wall and footwall, the coal seam close to the fault surface is pulled by stress and deforms. The fold size and the structural coal influence width expand gradually, and shear stress forms between the faults. The mechanical analysis of the structural coal formation in the two walls of a normal fault is shown in Figure 16. The presence of a normal fault provides a material basis for coal and gas outburst accidents, i.e., weak and broken structural coal. The residual structural stress also increases the risk of such accidents. This area has the material basis and power conditions for coal and gas outbursts.

4.2. *The Blasting Stress Wave Propagation within Normal Fault.* Because the wave impedance of coal is far less than that of rock, the stress wave is transmitted and reflected at the coal-rock interface, thereby producing the transmitted

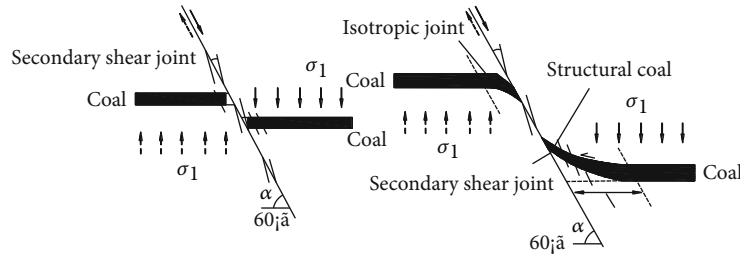


FIGURE 16: Mechanical analysis of structural coal in normal fault.

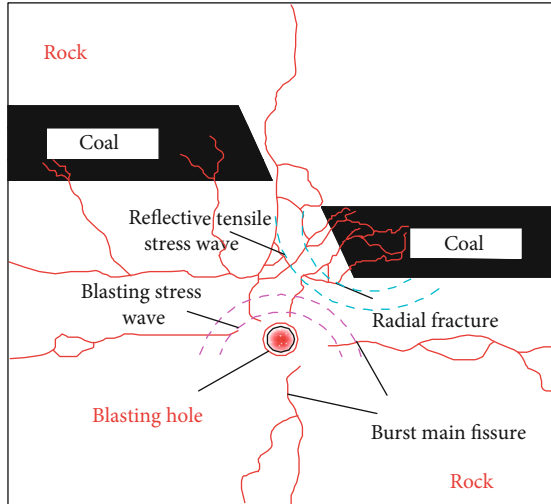


FIGURE 17: Propagation of blasting stress wave within normal fault.

compression wave and the reflected tension wave. Where the transmitted compression stress wave and the reflected tension stress wave pass, the coal and rock experience compression and expansion deformation, as shown in Figure 17.

Under the action of the blasting impact load, the stress waves first form microdamage and microcracks in the rock. Because of the reflection of the stress wave near the coal-rock interface, the transformation of compressive stress and tensile stress is frequent, and energy accumulates repeatedly [25]. The transmitted compressive stress wave acts on the coal body, thereby increasing the coal-seam cracks. The reflected tensile stress wave acts on the rock and causes a thorough crack in the rock near the coal body, thereby increasing the damage degree and range of the rock.

**4.3. The Effects on Coal and Gas Outbursts.** Cumulative damage due to blasting vibrations causes the most severe damage to the coal-rock interface in the upper wall of the normal fault. This provides a passage for gas and a weak surface for the occurrence of a dynamic gas disaster, which is conducive to the occurrence of a coal and gas outburst.

Before the coal and rock in normal fault disturbed by blasting dynamics, the free and adsorbed gases in the coal pores and fissures remain in dynamic equilibrium. However, when a tensile stress wave acts on the tectonic soft coal near the normal fault, the coal in this area expands and deforms, thereby increasing the pores and fissures. This destroys the adsorption equilibrium state within the coal body. The

adsorbed gas is desorbed into free gas that diffuses into the blasting crack area, thereby providing a dynamic basis for coal and gas outbursts and increasing the risk of these events.

The mechanical conditions leading to coal and gas outbursts depend on the tensile stress, gas pressure, and shear strength of the coal near the normal fault [25]. Penetrating cracks in the coal and rock between the blasting hole and the upper wall of the normal fault reduce the friction between the bedding planes inside the coal and the interfaces with the rock. Thus, when the tensile stress and gas pressure in the coal exceed the shear strength and friction force of the coal and rock, the gas internal energy stored in the coal seam and the coal elastic potential energy are released rapidly along the weak broken surfaces between the coal and rock [30, 31], thereby resulting in an outburst.

**4.4. Example of Coal and Gas Outburst.** On April 4, 2018, a large coal and gas outburst accident occurred in the vertical shaft of the Didaoshenghe Coal Mine of the Heilongjiang Longmei Jixi Mining Co., Ltd. (hereinafter referred to as the Didao shaft). The accident resulted in five deaths, with 67 t of coal being thrown out and a gas emission volume of  $\sim 2300 \text{ m}^3$ . The working face of the accident was the excavation face of the main roadway of the east mining in the second mining area of the Didao shaft (hereinafter referred to as working face 03).

During the roadway excavation process, coal seams 24 and 26 were exposed. The working face of roadway excavation involves blasting excavation and semicontinuous transportation. At the time of the accident, the working face had exposed coal seam 24 and was 3.5 m past the coal gate; the working face was located between normal faults F7 and F8. The accident site had a complex geological structure: the coal seam was soft and broken under the influence of the fault structure, and there was residual tectonic stress [32].

The direct causes of the accident were that (i) the regional outburst-prevention measures did not eliminate completely the risk of a coal outburst in the area of uncovered coal, (ii) the local outburst-prevention measures were imperfect, and (iii) the control range of some of the coal-uncovering measures was insufficient. The coal and gas outburst was induced by disturbances from air-powered coal drilling. The site of the outburst accident in the Didao shaft is shown in Figure 18, where Figure 18(a) shows working face 03 after the outburst. Figure 18(b) shows the roof of working face 03 after the outburst, Figure 18(c) shows the hole on the left side of working face 03 after the outburst,

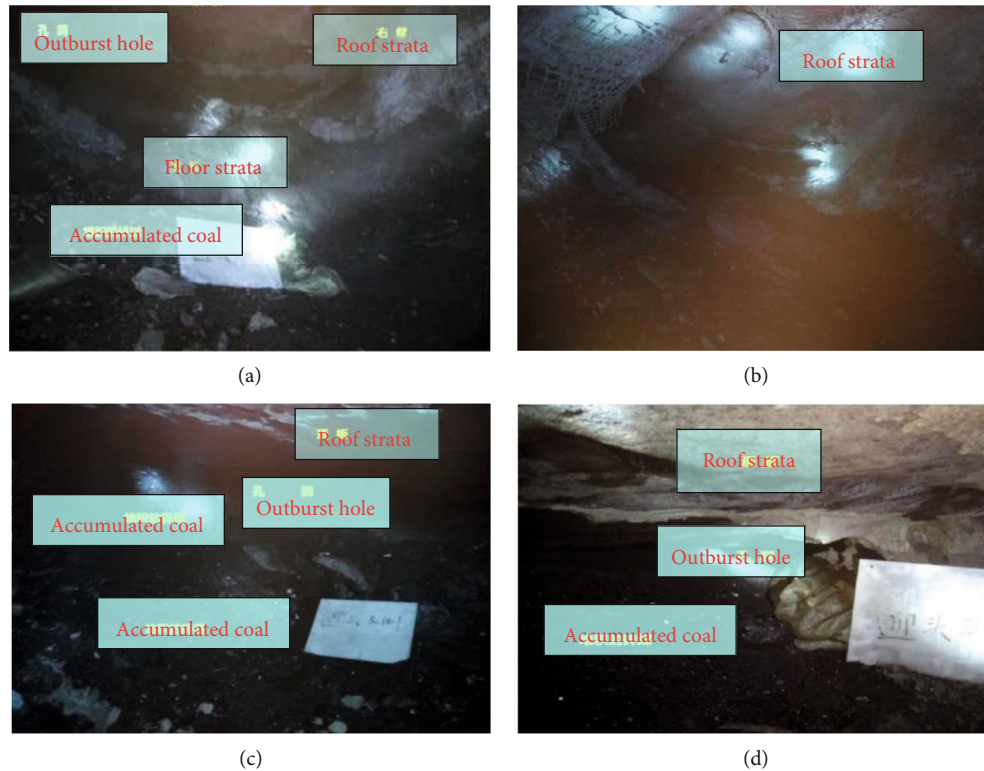


FIGURE 18: Photographs of coal and gas outburst in Didao Coal Mine (Heilongjiang Province, China): (a) working face; (b) roof of working face; (c) hole in left side of working face; (d) hole in right side of working face.

and Figure 18(d) shows the hole on the right side of working face 03 after the outburst. The coal seam in the area where the accident occurred was affected by the normal-fault structure to develop tectonic coal, thereby providing the basic material conditions for the occurrence of the coal and gas outburst.

The cumulative damage of blasting vibrations in the normal-fault structural area caused the most serious damage to the rock in the direction of the coal seam in the upper wall of the normal fault and the blast hole. The coal on the upper wall of the fault and the rock showed dense network cracks. The damage cracks provided a weak surface for the coal and gas outburst, and the developed cracks also provided a channel for gas flows. These were conducive to the occurrence of the coal and gas outburst accident. Because of the disturbance of the explosion stress wave, the expansion and deformation of the coal seam increased the transformation of adsorbed gas into free gas, the gas balance in the original coal seam was broken, and the gas pressure increased, which provided the dynamic conditions for a coal and gas outburst and increased the danger of one.

The accident occurred between normal faults F7 and F8, where the structural coal was developed. The residual structural stress and the further disturbance of the blast action reduced the strength of the coal body even more. The gas desorption promoted the increase of gas pressure in the coal seam. When pneumatic coal drilling disturbed the area affected by blasting within the normal-fault structure, the tensile stress and gas pressure in the coal seam were greater than the shear strength of the coal, and the high-pressure gas

expelled the broken coal rapidly from the weak surfaces, thereby leading to the coal and gas outburst accident.

## 5. Conclusions

We draw the following three conclusions from this study.

The blasting simulation experiment showed that the normal-fault structure and fault plane are affected greatly by blasting, and the layer of coal and rock between the blast hole and the upper wall is influenced the most by the blasting stress. In the model with a normal fault, the maximum tensile stress in the vertical direction of the blast hole is 1.17 times that in the model with no fault. The stress curve in the vertical direction of the blast hole in the normal-fault model is obviously more complicated. Meanwhile, the stress wave produces multiple transmissions and reflections in the normal-fault structural area, which cause serious damage to the coal-rock interface.

The numerical simulation results show that the propagation of the blasting stress wave in the normal-fault structural area is complicated, resulting in an obvious stress concentration at the fault plane in the upper wall of the normal fault. This is an important reason for the high density of cracks in the direction of the blast hole and the coal seam in the upper wall of the normal fault. Because of the accumulation of blast vibrations and the presence of the normal-fault structure, the destruction of the rock and coal seam near the coal fault area is accelerated. The strength of the coal and rock in the normal-fault structural area is reduced, and this is a potentially dangerous area for coal and gas outbursts.

The Didaoshenghe Coal Mine is located in a complex structural zone with a high density of faults and residual structural stress. Its coal seam is softened and broken under the influence of a normal-fault structure, which provides a material basis for outburst incidents. Blasting operations disturb the normal-fault structural area, and the cumulative damage of blast vibrations increases the extent and scope of damage to the coal and rock. Broken coal and rock provide weak surfaces and gas flow channels for the occurrence of dynamic gas disasters. The disturbances of coal drilling operations to blasting areas with normal faults constitute an important reason for coal and gas outburst incidents.

## Data Availability

The test data used to support the findings of this study are included within the article. Readers can obtain data supporting the research results from the test data table in the paper.

## Conflicts of Interest

The authors declare that they have no known competing financial interests or personal relationships that could have appeared to influence the work reported in this paper.

## Acknowledgments

This study was financially supported by the National Science Foundation of China (grant nos. 5207-4013 and 5160-4010) and Natural Science Foundation Project of Anhui Provincial Department of Education (grant no. KJ2020A0327). These funds are gratefully acknowledged.

## References

- [1] X. L. Li, Z. Y. Cao, and Y. L. Xu, "Characteristics and trends of coal mine safety development," *Energy Sources, Part A: Recovery, Utilization, and Environmental Effects*, pp. 1–19, 2020.
- [2] B. B. Beamish and P. J. Crosdale, "Instantaneous outbursts in underground coal mines: an overview and association with coal type," *International Journal of Coal Geology*, vol. 35, no. 1–4, pp. 27–55, 1998.
- [3] R. D. Lama and J. Bodziony, "Outbursts of gas, coal and rock in underground coal mines (1996)," *International Journal of Surface Mining, Reclamation, and Environment*, vol. 11, no. 3, p. 499, 1997.
- [4] H. W. Jin, Q. H. Gao, Q. H. Zhang, G. Xu, S. L. Yu, and J. Zhou, "Study on the shatter proneness and its test method of coal with high-pressure adsorbed gas," *Arabian Journal of Geosciences*, vol. 12, no. 17, pp. 1–10, 2019.
- [5] S. Valliappan and W. H. Zhang, "Role of gas energy during coal outbursts," *International Journal for Numerical Methods in Engineering*, vol. 44, no. 7, pp. 875–895, 1999.
- [6] D. D. Yang, Y. J. Chen, J. Tang et al., "Experimental research into the relationship between initial gas release and coal-gas outbursts," *Journal of Natural Gas Science and Engineering*, vol. 50, pp. 157–165, 2018.
- [7] Y. X. Cao, D. D. He, and D. C. Glick, "Coal and gas outbursts in footwalls of reverse faults," *International Journal of Coal Geology*, vol. 48, no. 1–2, pp. 47–63, 2001.
- [8] B. Chen, S. C. Zhang, Y. Y. Li, Z. K. Li, and H. J. Zhou, "Physical simulation study of crack propagation and instability information discrimination of rock-like materials with faults," *Arabian Journal of Geosciences*, vol. 13, no. 18, pp. 1–12, 2020.
- [9] H. Y. Li, "Major and minor structural features of a bedding shear zone along a coal seam and related gas outburst, Pingdingshan coalfield, northern China," *International Journal of Coal Geology*, vol. 47, no. 2, pp. 101–113, 2001.
- [10] M. B. Wold, L. D. Connell, and S. K. Choi, "The role of spatial variability in coal seam parameters on gas outburst behaviour during coal mining," *International Journal of Coal Geology*, vol. 75, no. 1, pp. 1–14, 2008.
- [11] X. W. Liu, Y. X. Cao, R. Liu, and D. D. He, "Bishordeninyl terpene alkaloids from *Zanthoxylum integrifolium*," *Journal of China Coal Society*, vol. 47, no. 3, pp. 571–574, 2000.
- [12] W. Yang, C. Z. Lu, G. Y. Si, B. Q. Lin, and X. D. Jiao, "Coal and gas outburst control using uniform hydraulic fracturing by distress blasting and water-driven gas release," *Journal of Natural Gas Science and Engineering*, vol. 79, article 103360, 2020.
- [13] K. Gao, P. Huang, Z. G. Liu, J. Liu, C. M. Shu, and G. D. Qiao, "Coal-rock damage characteristics caused by blasting within a reverse fault and its resultant effects on coal and gas outburst," *Scientific Reports*, vol. 11, no. 1, p. 19158, 2021.
- [14] H. Li, L. Tian, B. Huang et al., "Experimental study on coal damage subjected to microwave heating," *Rock Mechanics and Rock Engineering*, vol. 53, no. 12, pp. 5631–5640, 2020.
- [15] H. Li, S. Shi, B. Lin et al., "Effects of microwave-assisted pyrolysis on the microstructure of bituminous coals," *Energy*, vol. 187, p. 115986, 2019.
- [16] S. M. Liu, X. L. Li, D. K. Wang, and D. Zhang, "Experimental study on temperature response of different ranks of coal to liquid nitrogen soaking," *Natural Resources Research*, vol. 30, no. 2, pp. 1467–1480, 2021.
- [17] X. L. Li, S. J. Chen, Z. H. Li, and E. Y. Wang, "Rockburst mechanism in coal rock with structural surface and the microseismic (MS) and electromagnetic radiation (EMR) response," *Engineering Failure Analysis*, vol. 124, no. 6, article 105396, 2021.
- [18] X. L. Li, S. J. Chen, Q. M. Zhang, X. Gao, and F. Feng, "Research on theory, simulation and measurement of stress behavior under regenerated roof condition," *Geomechanics and Engineering*, vol. 26, no. 1, pp. 49–61, 2021.
- [19] X. L. Li, S. J. Chen, S. M. Liu, and Z. H. Li, "AE waveform characteristics of rock mass under uniaxial loading based on Hilbert-Huang transform," *Journal of Central South University*, vol. 28, no. 6, pp. 1843–1856, 2021.
- [20] B. S. Nie and X. C. Li, "Mechanism research on coal and gas outburst during vibration blasting," *Safety science*, vol. 50, no. 4, pp. 741–744, 2012.
- [21] C. J. Wang, S. Q. Yang, D. D. Yang, X. W. Li, and C. L. Jiang, "Experimental analysis of the intensity and evolution of coal and gas outbursts," *Fuel*, vol. 226, pp. 252–262, 2018.
- [22] J. Tang, C. L. Jiang, Y. J. Chen, X. W. Li, G. D. Wang, and D. D. Yang, "Line prediction technology for forecasting coal and gas outbursts during coal roadway tunneling," *Journal of Natural Gas Science and Engineering*, vol. 34, pp. 412–418, 2016.
- [23] S. Xue, Y. C. Wang, J. Xie, and G. Wang, "A coupled approach to simulate initiation of outbursts of coal and gas – model development," *International Journal of Coal Geology*, vol. 86, no. 2–3, pp. 222–230, 2011.

- [24] C. M. Mu and J. Qi, "Model investigation on cracks propagation in coal under blast loading," *Shock and Vibration*, vol. 31, no. 13, pp. 58–61, 2012.
- [25] S. C. Zhang, Z. G. Liu, J. Liu, W. Q. Zhang, and K. Gao, "Experimental study on similar material of simulating coal blasting," *Journal of Anhui University of Science and Technology (Natural Science)*, vol. 38, no. 2, pp. 1–6, 2018.
- [26] F. H. Zhu, *Study on the characteristics of damage and crack evolution under the shaped charge blasting*, Anhui University of Science and Technology, 2019, Dissertation.
- [27] K. Gao, Z. G. Liu, J. Liu, F. H. Zhu, G. D. Qiao, and S. C. Zhang, "Application research of directional cumulative blasting for weakening reverse faults in fully mechanized excavation face," *Chinese Journal of Rock Mechanics and Engineering*, vol. 38, no. 7, pp. 1408–1419, 2019.
- [28] J. Z. Bai, *LS-DYNA3D Theoretical Basis and Case Analysis*, Science Press, Beijing, 2005.
- [29] E. M. Anderson, *The Dynamics of Faulting and Dyke Formation with Applications to Britain*, Oliver and Boyd, Edinburgh, 1951.
- [30] F. H. An, Y. Yuan, X. J. Chen, Z. Q. Li, and L. Y. Li, "Expansion energy of coal gas for the initiation of coal and gas outbursts," *Fuel*, vol. 235, pp. 551–557, 2019.
- [31] W. Zhao, Y. P. Cheng, H. N. Jiang, K. Jin, H. F. Wang, and L. Wang, "Role of the rapid gas desorption of coal powders in the development stage of outbursts," *Journal of Natural Gas Science and Engineering*, vol. 28, pp. 491–501, 2016.
- [32] Incident Investigation Team, *Heilongjiang Longmei Jixi Mining Co., Ltd. Didaoshenghe Coal Mine Vertical Shaft "4-4" Large Coal and Gas Outburst Investigation Report*, Heilongjiang Coal Mine Safety Supervision Bureau, Heilongjiang, 2018.